Available online at www.sciencedirect.com
SCIENCE DIRECT®
Fire Safety Journal 40 (2005) 141–176
FIRE SAFETY JOURNAL
www.elsevier.com/locate/firesaf

A simplified model for soot formation and oxidation in CFD simulation of non-premixed hydrocarbon flames

Christopher W. Lautenberger[a,*], John L. de Ris[b], Nicholas A. Dembsey[a], Jonathan R. Barnett[a], Howard R. Baum[c]

[a]*Center for Firesafety Studies, Worcester Polytechnic Institute, Worcester, MA 01609, USA*
[b]*FM Global Research, 1151 Boston-Providence Hwy., Norwood, MA 02062, USA*
[c]*Building and Fire Research Laboratory, National Institute of Standards and Technology, Gaithersburg, MD 20899, USA*

Received 2 December 2003; received in revised form 22 June 2004; accepted 14 October 2004
Available online 6 January 2005

Abstract

A new approach to modeling soot formation and oxidation in non-premixed hydrocarbon flames has been developed and subjected to an initial calibration. The model considers only the phenomena essential for obtaining sufficiently accurate predictions of soot concentrations to make CFD calculations of fire radiation feasible in an engineering context. It is generalized to multiple fuels by relating the peak soot formation rate to a fuel's laminar smoke point height, an empirical measure of relative sooting propensity, and applying simple scaling relationships to account for differences in fuel stoichiometry. Soot oxidation is modeled as a surface area independent process because it is controlled by the diffusion of molecular oxygen into the zone of active soot oxidation rather than being limited by reaction of $OH\cdot$ radicals with the available soot surface area. The soot model is embedded within a modified version of NIST's Fire Dynamics Simulator and used for a comparison of predicted and measured temperatures, soot volume fractions, and velocities in laminar ethylene, propylene, and propane flames. The

*Corresponding author. Department of Mechanical Engineering, University of California, 60A Hesse Hall, Berkeley, CA 94720, USA. Tel.: +1 540 643 5282; fax: +1 540 642 1850.
E-mail address: clauten@me.berkeley.edu (C.W. Lautenberger).

doi:10.1016/j.firesaf.2004.10.002

Nomenclature

A_f	flame surface area (m^2)
B_R	soot constant (dimensionless)
c_p	constant-pressure specific heat (kJ/kg K)
C_2	Planck's second constant (m K)
$C_{\kappa R}$	constant relating f_v and T to κ_s [$(m K)^{-1}$]
D	diffusivity (m^2/s)
f	mixture fraction soot formation function ($kg/m^3 s$)
f_v	soot volume fraction (m^3 soot/m^3 mixture)
g	temperature soot oxidation function (dimensionless)
$\boldsymbol{g}$	acceleration of gravity vector (m/s^2)
h	sensible enthalpy (kJ/kg)
h°	enthalpy of formation (kJ/kg)
h_T	total enthalpy ($h + h^\circ$) (kJ/kg)
ΔH_c	heat of combustion (kJ/kg)
k	thermal conductivity (W/m K)
ℓ_s	laminar smoke point height (m)
ℓ_f	flame height (m)
L	pathlength, mean bean length (m)
M	molecular weight of a single species (kg/mol)
$\overline{M}$	mean molecular weight of a gas mixture; $\overline{M} = (\Sigma Y_i/M_i)^{-1}$ (kg/mol)
N	soot number density (particles/m^3)
p°	reference pressure (101,300 Pa)
p_0	background pressure (Pa)
Pr	Prandtl number (dimensionless)
$\dot{Q}$	heat release rate (W or kW)
Q	volumetric flow rate (cm^3/s)
R	universal gas constant (8.314 J/mol K)
S	Stoichiometric oxidant to fuel mass ratio (dimensionless)
Sc	Schmidt number (dimensionless)
T	temperature (K)
$\boldsymbol{u}$	velocity vector (m/s)
V	velocity (m/s)
X	mole fraction (dimensionless)
Y	mass fraction (dimensionless)
Z	mixture fraction (dimensionless)

Greek symbols

κ	emission/absorption coefficient (m^{-1})
λ	wavelength (μm)
μ	viscosity (kg/m s)
v	Stoichiometric coefficient (dimensionless)

ρ	density, general (kg/m^3)
ρ_2	density, two-phase (kg/m^3)
ρ_g	density, gas-phase (kg/m^3)
σ	Stefan–Boltzmann constant ($5.67 \times 10^{-8}\,W/m^2\,K^4$)
τ	characteristic time (s)
$\boldsymbol{\tau}$	viscous stress tensor ($kg/m\,s^2$)
χ	local nonadiabaticity (dimensionless)
χ_r	global radiative fraction (dimensionless)
ψ	multiplying factor in mixture fraction soot polynomials, equal to Z/Z_{st} (dimensionless)
$\dot{\omega}$	formation rate (kg/s)

Subscripts

f	flame
F	fuel
g	gas or gas-phase
H	high
i	species *i*
L	low
P	peak
r	radiation
s	soot, smoke point, stoichiometric mass ratio
sp	smoke point
so	soot oxidation
sf	soot formation
st	stoichiometric
T	transferred
∞	ambient

Superscripts

$(\,)''$	per unit area
$(\,)'''$	per unit volume
$\dot{(\,)}$	per unit time

Abbreviations

Exp.	experimental
FDS	fire dynamics simulator
HAB	height above burner
HRR	heat release rate
ID	inner diameter
PAH	polycyclic aromatic hydrocarbon
Pred.	Predicted

basic approach, though promising, is not yet mature and several suggestions for future work are presented.

Keywords: Soot; Soot formation; Soot oxidation; Smoke point; Non-premixed combustion; Diffusion flames; Computational fluid dynamics; Fire dynamics simulator; Flame radiation

1. Introduction

Computational Fluid Dynamics-based fire models are particularly well suited for the study of fire behavior. However, most codes need further development and validation against experiment in the areas of soot formation and oxidation before they can be used to reliably predict flame heat transfer, the burning of condensed fuels, and fire growth. Continuum thermal radiation from soot particles accounts for the majority of flame radiation, with spectral gas radiant emission being less important in all but lightly sooting fuels. Therefore, a realistic description of the evolution of soot through the flame envelope is one of the many components necessary to accurately calculate radiation from non-premixed flames. Consequently, a fire model's treatment of soot formation and oxidation has a profound influence on its predictions of mass burning, flame spread, and fire growth because at hazardous scales these processes are driven by thermal radiation. However, no universal soot model exists, and most of the previously developed soot models are impractical for use in fire safety engineering due to their complexity, computational cost, or large number of fuel-specific parameters that are not easily obtained.

In this paper, experimental findings are exploited in the development of a new approach to modeling soot formation and oxidation in non-premixed (diffusion) flames. The new soot model is incorporated within a modified version of NIST's Fire Dynamics Simulator (FDS) [1,2] and used to predict soot formation/oxidation and radiation from laminar non-premixed flames by direct numerical simulation (DNS). By generalizing the model to multiple fuels and keeping its computational cost to a minimum, the new soot model is appropriate for use in fire safety engineering where a variety of fuels are encountered and long calculation times are often impractical for hazard analysis or design purposes.

2. Soot formation in non-premixed flames and its relation to the laminar smoke point

There exists a large body of scientific literature on the chemical mechanisms of soot formation in non-premixed flames. As discussed in Appendix A, there is evidence for at least two mechanisms of soot formation: (1) Hydrogen Abstraction with acetylene (i.e., Carbon) Addition (HACA) to the available surface area of the growing soot particles, and (2) addition of polycyclic aromatic hydrocarbons (PAHs). These competing mechanisms are distinctly different because the HACA mechanism is controlled by heterogeneous surface reactions whereas the PAH

mechanism is controlled by homogeneous gas-phase reactions. These chemistry issues are complex and still far from resolution.

Fortunately, from an engineering standpoint, the problem of soot formation in non-premixed flames is made tractable by their inherent simplicity. The location of the flame front and peak temperature is controlled by the stoichiometry of the reactants rather than complex chemical kinetics that govern premixed flames. Overall heat release rates are controlled by diffusion of reactants to a thin flame sheet separating the fuel from the oxidant. Diffusion times are much greater than chemical kinetic reaction times which govern local heat release rates, and the simplicity created by this large ratio of times is the basis for the success of the Shvab-Zel'dovitch [3] model of non-premixed flames. It also underlies Bilger's success [4] in correlating concentrations of major species in terms of the local mixture fraction (the local fraction of mass in the gas-phase that originated in the fuel stream) across non-premixed flames for a wide range of overall flame heat-release rates. Since the soot formation/oxidation times in non-premixed flames are much greater than the main heat release reaction times, one need only consider the diffusion times and soot formation/oxidation times, while regarding the main heat release chemical reaction time as being instantaneous.

In non-premixed flames, each set of reactants (i.e., fuel and oxidant) provides a unique chemical environment for the formation of soot. What varies from flame to flame for a given set of reactants is the ratio of the soot formation/oxidation time to the diffusion (i.e., flow) time. One can quantify this ratio for a particular fuel by considering its buoyant laminar "candle-like" flame burning in air. Increasing the flame height increases the residence time and allows more time for the flame to produce soot. Once formed, this soot requires additional time to oxidize in the upper parts of the flame if it is to be entirely consumed below the flame tip. As soot travels through the flame (in a Lagrangian sense), it radiates away energy and cools the flame gases. At the "smoke point" flame height, radiative heat loss from the flame approaches 30% of the total heat release [5], flame gases have cooled just sufficiently to prevent further oxidation of soot, and the soot formation/oxidation time becomes equal to the diffusion time. A fuel's smoke point is the maximum height of its laminar flame burning in air at which soot is not released from the flame tip. It is a unique measure of a hydrocarbon fuel's sooting propensity and has long been used by aviation engineers as an empirical measure of a fuel's relative sootiness [6]. In this work, the smoke point is introduced as the single most important "fuel property" for an engineering model of soot formation.

There is a large body of literature establishing correlations between the smoke point and soot formation or flame radiation in non-premixed hydrocarbon flames. This literature includes: (1) correlation of the peak soot volume fraction and characteristic soot formation growth rates of buoyant laminar flames at their smoke point [7–10]; (2) peak soot volume fractions of turbulent buoyant fuel jets [11] and turbulent pool fires [12]; (3) radiant fractions from buoyant turbulent fuel jets [13]; (4) incompleteness of combustion from small-diameter pool fires [14]; and (5) smoke release from turbulent buoyant flames [15]. Rules for the smoke point of mixtures of hydrocarbons in terms of the components have been developed for both liquid [16]

and gaseous fuels [17]. A conceptual understanding of the smoke point mechanism [7] combined with knowledge of its pressure dependence [18] formed the basis for successfully predicting the pressure dependence of radiation from both laminar and turbulent flames [19]. Of perhaps greater significance is the development of general correlations of radiation from both laminar [5,17] and turbulent [20] non-premixed flames in terms of only the smoke point of the supplied fuel mixture, the stoichiometric oxidant to fuel mass ratio, and the adiabatic stoichiometric flame temperature of the reactants. The latter correlations hold over the full range of tested ambient oxygen concentrations. Tewarson [21] summarizes use of the smoke point for predicting fire properties of gaseous, liquid, and solid fuels.

The general consistency of these correlations based on the smoke point is striking: no crossovers in ranking are observed. For engineering purposes, once the smoke point of the fuel, stoichiometric mass ratio of the reactants, and adiabatic stoichiometric flame temperature are known for a given set of reactants, the release of soot and radiation may be obtained from available correlations. From a combustion engineering viewpoint, these three quantities summarize the essential fundamental combustion properties of the non-premixed fuel/oxidant system. These arguments are based almost solely on empirical evidence. As such, it is hard to know their limitations. To fully establish the proposed simplified concept for non-premixed flames, one must have a mathematical model to examine its assumptions, quantify its limitations, and make predictions for untested situations of both scientific and practical interest. This is the subject of the following sections where a new soot model based on the smoke point is introduced and used to calculate soot formation and oxidation in small-scale flames of several fuels. Although the model is applied only to small laminar flames in this paper, it can be applied to large eddy simulations of larger turbulent flames using statistical probability density function methods to account for unresolved subgrid-scale fluctuations. The required mathematics and a demonstration of an earlier version of the current soot model applied to LES of a 100 kW buoyant turbulent diffusion flame are presented in Appendices B and J of Lautenberger [22].

3. A new approach to modeling soot formation in non-premixed flames

We have attempted to develop a model for soot formation and oxidation that considers only the phenomena essential for obtaining sufficiently accurate predictions of soot concentrations to make CFD calculations of flame radiation from non-premixed flames of an arbitrary hydrocarbon fuel feasible, thereby retaining simplicity and minimizing computational expense. Future work that compares model predictions with experimental heat flux measurements should allow one to establish what constitutes a sufficiently accurate prediction. Appendix A provides support to the current modeling approach by giving a brief review of soot formation and oxidation in non-premixed flames, and describing the experimental data and soot formation/oxidation theories that were contemplated during development of the new model.

The postulated model deviates from the classical view of soot formation and oxidation because processes of nucleation, inception, coagulation, and agglomeration are not explicitly considered. This minimizes computational expense because it avoids solving a conservation equation for the soot particle-number density. The basic form of the soot model was inspired by the work of Kent and Honnery [23]. They correlated soot growth rates with mixture fraction and temperature in laminar ethane and ethylene flames by combining the mixture fraction and velocity fields obtained from numerical flame simulations with experimental soot and temperature measurements. The result was a parametric soot model with which the soot formation rate could be estimated from only the local mixture fraction and temperature. However, this model was applicable only to ethane and ethylene, and used detailed experimentally determined soot formation maps.

In the proposed model, soot formation and oxidation rates are calculated as analytic functions of mixture fraction and temperature. The model is generalized to multiple hydrocarbon fuels by relating a fuel's peak soot formation rate to its laminar smoke point height and applying simple scaling relationships to account for differences in fuel stoichiometry. It is not necessary to establish fuel-specific model constants because the smoke point height has been measured for many fuels, including gases, liquids, and solids [24]. The model assumes that the "bands" of mixture fraction space over which soot formation and oxidation occur are identical for all fuels when normalized by the stoichiometric value of mixture fraction. This bold simplification neglects any details in fuel-specific chemistry not already incorporated in the smoke point or fuel stoichiometry.

Of all the soot models in the literature, the current model is perhaps most similar to the two equation model of Moss and Stewart [25]. Their soot formation model contains simple expressions for quantifying particle nucleation, surface growth, and coagulation; it uses three fuel-specific empirical constants that control the rates of each of these three processes. The rate of nucleation and surface growth are linearly proportional to the concentration of a "critical precursor species". This is taken as the total hydrocarbon mole fraction as determined from a detailed chemistry numerical simulation of a counterflow flame and tabulated as a function of mixture fraction. In this way, the rate of inception and surface growth become functions of mixture fraction and temperature, as in the present model. Soot oxidation is attributed to OH and treated as a surface area dependent process.

There are several critical differences between the new model presented here and that of Moss and Stewart [25]. First, the specific soot surface area is neglected in both the formation and oxidation source terms. This eliminates the need to solve a separate conservation equation for the soot number density, reducing the computational cost of the soot model by approximately 50%. Second, soot formation is not attributed to the presence of precursor species; rather, it is specified as an explicit function of mixture fraction without consideration of the parent fuel beyond differences in stoichiometry. Third, there are no fuel-specific constants; the laminar smoke point height is used to account for differences in sooting behavior of different fuels.

3.1. Basic model formulation

As discussed in Appendix A, it is likely that both heterogeneous (surface area-dependent) and homogeneous (surface area-independent) soot formation processes contribute to the total soot formation rate in non-premixed hydrocarbon flames. Heterogeneous processes are more important in lightly sooting flames than in heavily sooting flames. In order to retain simplicity and reduce the number of adjustable constants, the model postulated here considers only homogeneous (volumetric) soot formation because most fuels of interest to fire protection engineers are moderately to heavily sooting, with the notable exception of lower alkanes, alcohols, and some cellulosics. This model is not capable of reproducing the blue zone that occurs in lightly sooting flames without a modification to suppress soot formation at short flame residence times low in the flame.

Soot oxidation is treated by a global, fuel-independent mechanism that is a function of mixture fraction and temperature. Although soot oxidation has traditionally been modeled as a surface area-dependent process, in this work it is modeled as a homogeneous process because diffusion of molecular oxygen is apparently the controlling process. As discussed in Appendix A, the experimentally observed [7–11] similarity of axisymmetric diffusion flames at their smoke points corroborates the claim here that soot oxidation is controlled by the diffusion of molecular oxygen rather than the surface area of soot. If the surface area were controlling, the observed similarity would never be achieved for the wide range of tested fuel smoke points. A recent numerical modeling study has established the inadequacy of traditional surface area-dependent models for soot oxidation [26].

The net rate of soot formation $\dot{\omega}_s'''$ (kg/m^3 s) is calculated as

$$\dot{\omega}_s''' = \dot{\omega}_{sf}''' + \dot{\omega}_{so}''' \tag{1}$$

The soot formation and oxidation rates in Eq. (1) are determined from the product of an analytic function of mixture fraction and an analytic function of temperature

$$\dot{\omega}_{sf}''' = \dot{f}_{sf}'''(Z) g_{sf}(T), \tag{2}$$

$$\dot{\omega}_{so}''' = \dot{f}_{so}'''(Z) g_{so}(T). \tag{3}$$

In Eqs. (2) and (3), $\dot{f}_{sf}'''(Z)$ and $\dot{f}_{so}'''(Z)$ have units of kg soot/(m^3 mixture s). The temperature functions, $g_{sf}(T)$, and $g_{so}(T)$, are dimensionless factors that account for the temperature-dependency of soot formation and oxidation, respectively. Several analytic forms of these functions were considered. General polynomials were selected due to their ability to approximate a variety of shapes.

3.2. Analytic soot formation functions

Experimental measurements were consulted for guidance in selecting the general shapes of the soot formation and oxidation functions. Kent and Honnery [27] give a soot formation rate map for a laminar ethylene diffusion flame in which the volumetric rate of soot formation [kg soot/(m^3 mixture s)] is plotted in terms of

mixture fraction and temperature. This map is analogous to $\dot{f}'''_{sf}(Z)g_{sf}(T) + \dot{f}'''_{so}(Z)g_{so}(T)$ in Eqs. (2) and (3). The soot formation rates [27] show an approximately parabolic trend in mixture fraction and a less-discernable trend in temperature, but also approximately parabolic. Peak soot formation rates occur at mixture fraction values between 0.10 and 0.15, and over the temperature range 1500–1600 K. The stoichiometric mixture fraction for ethylene burning in air is 0.0629.

Consistent with the trends discussed above, the analytic soot formation mixture fraction function $\dot{f}'''_{sf}(Z)$ was chosen as a polynomial that rises from a formation rate of zero at a mixture fraction of Z_L to a peak formation rate at a mixture fraction of Z_P and then falls back to zero at a mixture fraction of Z_H. The polynomial was forced to be third order (four coefficients). Its coefficients are determined by specifying Z_L, Z_P, Z_H, and $\dot{f}'''_{sf}(Z_p)$ and then solving the resultant set of linear equations. Fig. 1 shows typical shapes of the mixture fraction polynomials. In order to generalize the model to multiple fuels, the values of Z_L, Z_P, and Z_H for each polynomial are related to the fuel's stoichiometric mixture fraction Z_{st} (between 0.05 and 0.10 for most fuels in air) by a parameter ψ of order unity. As an example, $Z_P = \psi_{sf,Z_P} Z_{st}$ is the mixture fraction value at which the peak soot formation rate occurs. These ψ constants are normalized mixture fraction values and are assumed fuel-independent (see Section 5).

The analytic soot formation temperature function $g_{sf}(T)$ was selected as a third order polynomial normalized between zero and unity. It takes on a value of zero at T_L, rises to a peak value of 1 at T_P, and falls back to 0 at T_H. T_L can be interpreted as

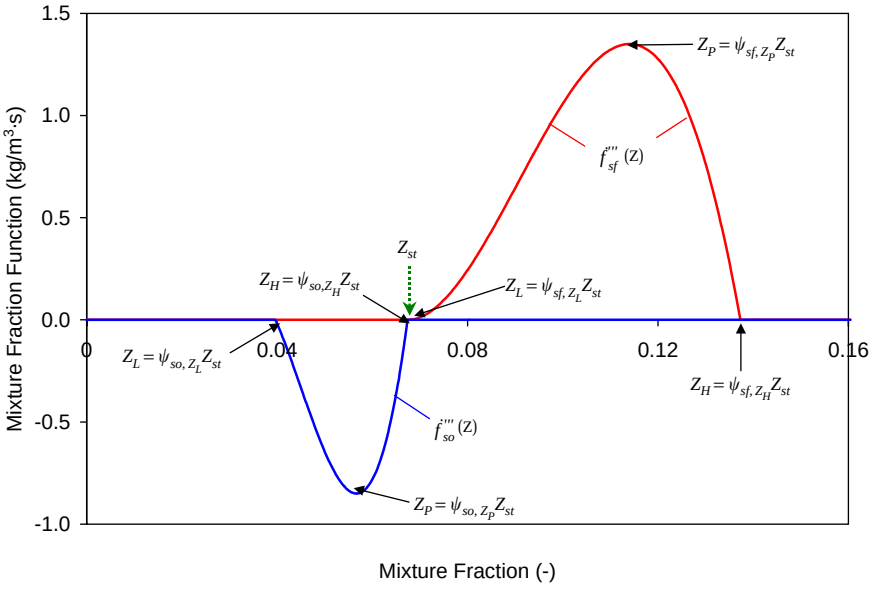

Fig. 1. Mixture fraction polynomials.

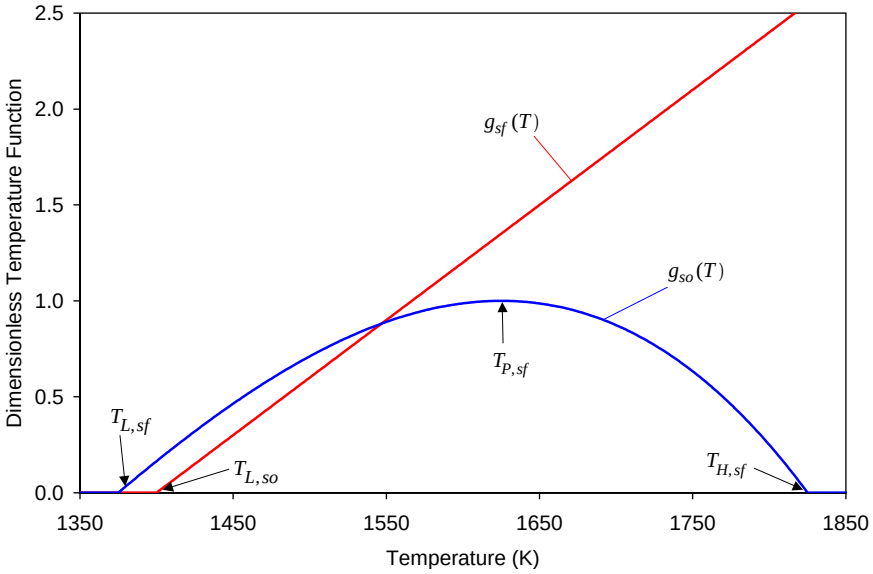

Fig. 2. Dimensionless temperature polynomials.

the minimum temperature at which soot forms, T_P is the temperature at which the soot formation rate reaches its peak, and T_H is the temperature above which no soot forms. Typical shapes of the temperature functions are given in Fig. 2.

3.3. Analytic soot oxidation functions

Soot oxidation in non-premixed flames is controlled by the diffusion of oxygen into the zone of active soot oxidation rather than being controlled by the reaction of $OH\cdot$ radicals impinging on the available soot surface area. Neoh et al. [28] demonstrated the importance of soot oxidation by $OH\cdot$ radicals and concluded that it was the principal oxidant under the conditions studied. Measurements of Puri et al. [29,30] show that the $OH\cdot$ concentration decreases strongly in the presence of oxidizing soot particles. The measurements also show that molecular oxygen concentrations remain very small in regions of active soot oxidation. The paucity of oxygen suggests that soot oxidation in non-premixed flames is controlled by the diffusion of oxygen into the soot oxidation zone at temperatures high enough for the oxygen to react with $H\cdot$ to form $OH\cdot$ radicals. Soot oxidation should therefore occur at values of mixture fraction where $OH\cdot$ is present. The range of mixture fractions relative to the stoichiometric mixture fraction is found from the measurements reported by Smyth [31] for a methane flame on a Wolfhard–Parker burner which show that peak $OH\cdot$ concentrations occur slightly to the oxidant side of stoichiometric. This was used as guidance for placing the soot oxidation function in mixture fraction space. The final location of the oxidation reaction in mixture

fraction space and its magnitude were determined through the laminar flame calibration exercise described in Section 5. No attempt was made to account for the effect of a fuel's H:C ratio on $OH\cdot$ concentrations or to account for the change of collision efficiency between $OH\cdot$ and soot particles as they age.

Similar to the soot formation functions, the soot oxidation mixture fraction function falls from a value of zero at Z_L to its peak negative value at Z_P, and then rises to a value of zero at Z_H. For simplicity, the oxidation rate was assumed linearly proportional to temperature, with no oxidation occurring below a critical value. The maximum soot oxidation rate calculated by the model may therefore be stronger than the "peak" oxidation rate because the soot oxidation temperature function may take on values greater than unity, whereas the formation temperature function is normalized between zero and one. A typical mixture fraction oxidation function is shown in Fig. 1, and a dimensionless soot oxidation temperature function is shown in Fig. 2.

4. Incorporating the new soot model with FDS

The soot model described conceptually above was incorporated within a modified version of FDS[1,2]. NIST's FDS[1,2] does not explicitly solve the energy equation, but uses it to determine the divergence of the velocity field. Here, instead, we explicitly solve an energy equation for the total (chemical plus sensible) gas-phase enthalpy, h_T and soot enthalpy, h_s. This simplifies the inclusion of temperature dependent specific heats and the evaluation of the local temperature in terms of the local enthalpy and mixture fraction. In the absence of soot and radiation, h_T is a conserved scalar depending only on the local mixture fraction. However in the presence of soot and flame radiation h_T is no longer a conserved scalar because a parcel of fluid experiences the accumulated effect of prior heat loss by radiation and change in sensible energy from the formation and oxidation of soot. The local temperature is evaluated from the gas-phase enthalpy and mixture fraction. This temperature is then used with the equation of state to evaluate the divergence of the velocity field and the resulting dilation that drives the buoyant flow.

The governing equations solved by the modified code are summarized in Eqs. 4–20. The kinematic viscosity is calculated as a function of mixture fraction and temperature for a multi-component fluid. Gaseous species and enthalpy diffusivity is inferred from the viscosity ($\rho_g D = \mu/\mathrm{Sc}$) by assuming a Schmidt number equal to 0.9 and unit Lewis number ($\mathrm{Pr} = \mathrm{Sc}$). The diffusion of soot occurs exclusively by thermophoresis. Soot is treated as the second phase of a two-phase fluid. It remains, however, in local thermal equilibrium with the gas. To simplify the model, soot is assumed to have the same C:H ratio as the supplied fuel. Fuel releases its heat of formation into the gas-phase during the formation of soot. Soot releases its heat of combustion while it is oxidized.

Both soot formation and flame radiation are very sensitive to temperature; so it must be computed accurately. One achieves good agreement with flame temperature measurements [31] by assuming the products of combustion consist only of H_2O and

CO_2 and providing a small enthalpy correction that transfers energy from the fuel side to the oxidant side near the flame sheet to account for the net diffusion of highly energetic low molecular weight species diffusing from the fuel side to the oxidant side of the flame [22].

Soot formation reaction

$$C_x H_y(g) \rightarrow C_x H_y(s) + M_F \Delta H_{sf}. \tag{4}$$

Fuel and soot oxidation reactions

$$C_x H_y + \nu'_{O_2} O_2 \rightarrow \nu''_{CO_2} CO_2 + \nu''_{H_2O} H_2O + M_F \Delta H_c. \tag{5}$$

Conservation of mass

$$-\frac{1}{\rho_g}\frac{D\rho_g}{Dt} = \nabla \cdot \boldsymbol{u} = \left(\frac{DZ}{Dt}\left.\frac{\partial T}{\partial Z}\right|_{h_T} + \frac{Dh_T}{Dt}\left.\frac{\partial T}{\partial h_T}\right|_Z\right) - \frac{1}{\overline{M}}\frac{DZ}{Dt}\frac{\mathrm{d}\overline{M}}{\mathrm{d}Z}. \tag{6}$$

Conservation of momentum

$$\rho_g\left(\frac{\partial \boldsymbol{u}}{\partial t} + (\boldsymbol{u}\cdot\nabla)\boldsymbol{u}\right) + \nabla p = \rho_g \boldsymbol{g} + \nabla \cdot \boldsymbol{\tau}. \tag{7}$$

Conservation of soot

$$\frac{\partial(\rho_2 Y_s)}{\partial t} + \boldsymbol{u}\cdot\nabla\rho_2 Y_s + \rho_2 Y_s \nabla \cdot u = 0.55\nabla \cdot \frac{Y_s \mu}{T}\nabla T + \dot{\omega}'''_s. \tag{8}$$

Conservation of mixture fraction

$$\frac{\partial(\rho_g Z)}{\partial t} + \boldsymbol{u}\cdot\nabla\rho_g Z + \rho_g Z \nabla\cdot\boldsymbol{u} = \nabla\cdot\rho_g D\nabla Z + \dot{\omega}'''_Z. \tag{9}$$

Conservation of total enthalpy

$$\begin{aligned}\frac{\partial(\rho_g h_T + \rho_2 Y_s h_s)}{\partial t} + \nabla\cdot(\rho_g h_T \mathbf{u} + \rho_2 Y_s h_s \mathbf{u}) &= \nabla\cdot\left(\rho_g D\nabla h_T + 0.55\frac{h_s Y_s \mu}{T}\nabla T\right)\\ &+ \dot{\omega}'''_{sf}(h_f - h_s) + \frac{\dot{\omega}'''_{so}}{M_F}(M_F h_s + M_{O_2}\nu'_{O_2} h_{O_2} - M_{CO_2}\nu''_{CO} h_{CO_2}\\ &- M_{H_2O}\nu''_{H_O} h_{H_2O}) - \dot{q}'''_r.\end{aligned} \tag{10}$$

Definition of total gas enthalpy

$$h_T(T) = \sum_i Y_i\left(h_i^\circ + \int_{T_0}^{T} c_p(T)\,\mathrm{d}T\right). \tag{11}$$

Ideal gas equation of state

$$\rho_g = \frac{p_0 \overline{M}}{RT}. \tag{12}$$

Two-phase (total) density

$$\rho_2 = \frac{\rho_g}{1 - Y_s}. \tag{13}$$

Loss (gain) of mixture fraction with the formation (oxidation) of soot

$$\begin{aligned} \dot{\omega}_Z''' &= -\dot{\omega}_{sf}''' \quad \text{(soot formation)} \\ \dot{\omega}_Z''' &= \frac{M_F}{\nu'_{O_2} M_{O_2} + M_F} \dot{\omega}_{so}''' \quad \text{(soot oxidation).} \end{aligned} \tag{14}$$

Radiant heat loss in Eq. (10) is given by

$$\dot{q}_r''' = 4\kappa\sigma T^4, \tag{15}$$

where the absorption coefficient, κ, is the sum of gas-phase and soot contributions

$$\kappa = \kappa_g + \kappa_s. \tag{16}$$

The gas absorption coefficient, κ_g, is evaluated prior to the main calculation in terms of the local temperature and mixture fraction using the narrow band radiation model, RADCAL [32]

$$\kappa_g(Z,T) = \int_{1\ \mu m}^{200\ \mu m} \kappa(T, L, P_{H_2O}, P_{CO_2} P_F, \lambda)\, d\lambda, \tag{17}$$

where the partial pressures of water vapor, carbon dioxide, and fuel (P_{H_2O}, P_{CO_2}, and P_F) are calculated from the background pressure p_0 and the mole fractions of each species as determined from the complete combustion state relations. The pathlength L in Eq. (17) is the mean beam length, which for the present tall laminar flames is twice the characteristic radius of the flames and scales according to [19]

$$L = 2r_f = 8.13 \left(\frac{D_\infty^2 \ell_f}{g} \right)^{1/4}, \tag{18}$$

where D_∞ is the ambient diffusivity.

For most fuels, the gas phase contribution to the total absorption coefficient is an order of magnitude less than that attributed to presence of soot particles. The spectral absorption–emission coefficient, $k_{s\lambda}$, of soot in the small particle limit is proportional to the soot volume fraction divided by the wavelength λ

$$k_{s\lambda} = \frac{B_s f_v}{\lambda}, \tag{19}$$

where B_s is a dimensionless constant. The proportionality constant B_s becomes 4.9 for the soot complex index of refraction $m = 1.57 - 0.56i$ that is commonly used for reporting soot volume fraction measurements in flames. Eq. (19) is valid for a discrete wavelength, but soot emits over all wavelengths. Integrating the soot emission over all wavelengths, Tien et al. [33] obtain the following expression for the soot absorption–emission coefficient

$$\kappa_s = 3.6 B_R f_v T / C_2 = C_{\kappa R} f_v T, \tag{20}$$

where C_2 is Planck's second constant. Eq. (20) was used in this work with $C_{\kappa R} = 1226\ (\text{mK})^{-1}$, consistent with $B_R = 4.9$ and how experimental measurements are usually reported.

5. Initial model calibration for a single ethylene flame

A calibration exercise was performed to determine the optimal soot model parameters for a 212 W laminar axisymmetric non-premixed ethylene flame [31] burning on a 1.1 cm diameter fuel tube with an 87 mm/s coflowing air stream. That is, the soot model constants were adjusted until optimal agreement between prediction and experiment was obtained. DNS simulations were performed with cylindrical coordinates using a grid spacing of 0.25 mm in the radial direction and 0.5 mm in the axial direction. Simulations performed with a finer mesh showed little variation, and thus the current results are considered grid-independent. A comparison between the measured temperature, soot volume fraction, and velocity profiles and the optimized model predictions is presented in Figs. 3–6. Eq. (21) was used to calculate the soot volume fraction profiles from the soot mass fractions (Eq. (8)) where the soot density is assumed to be $\rho_s = 1800\ \mathrm{kg/m^3}$

$$f_v = \frac{\rho_2 Y_s}{\rho_s}. \tag{21}$$

Based on these simulations, a set of global parameters is suggested. The (fuel-independent) ψ values that yielded optimal agreement between prediction and experiment are given in the first three rows of Table 1. Recall that the ψ values are used to establish the fuel-independent ranges of normalized mixture fraction over which soot formation and oxidation is assumed to occur. Also given in Table 1 is the peak soot formation and oxidation rates that provided the best agreement, denoted

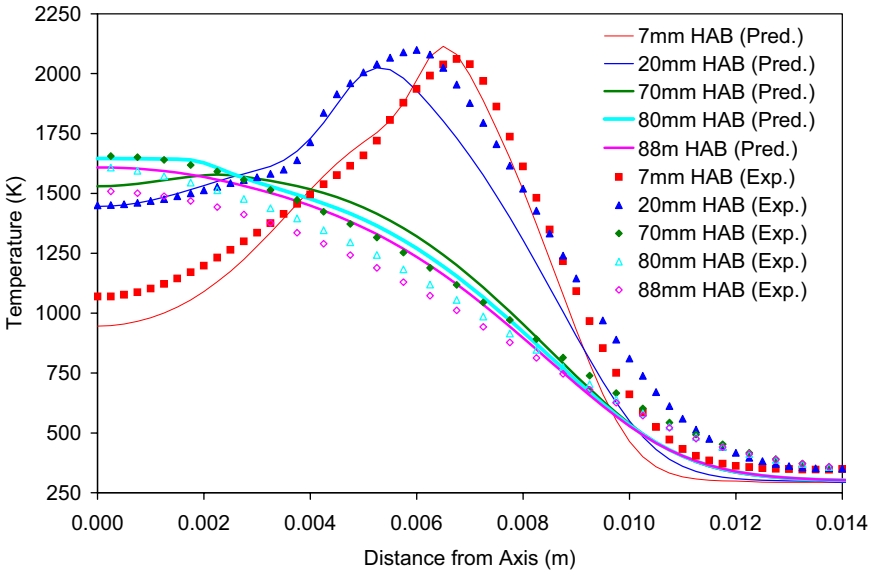

Fig. 3. Optimal temperature predictions in 212 W ethylene flame at several heights above burner (HAB).

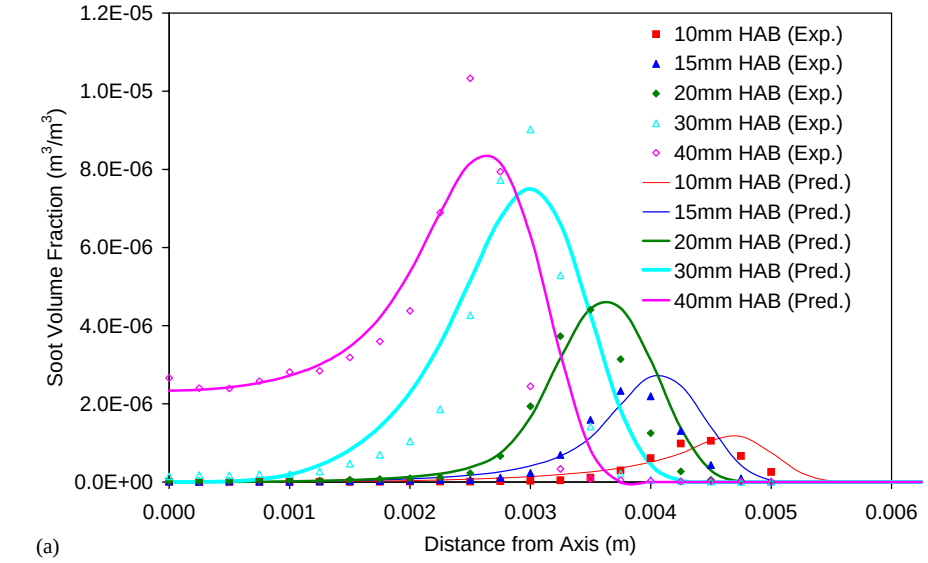

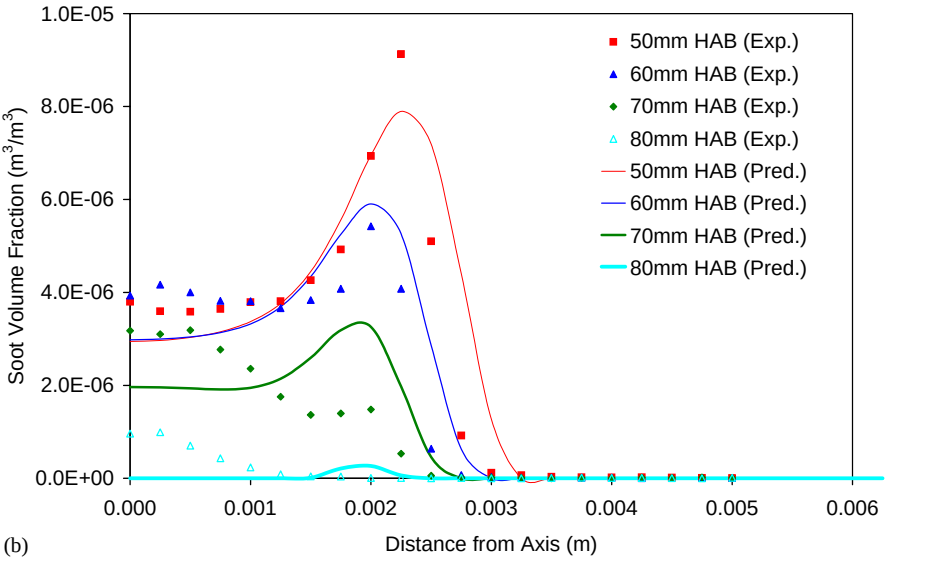

Fig. 4. Optimal f_v predictions in 212 W ethylene flame at several heights above burner (HAB): (a) 10–40 mm, (b) 50–80 mm.

as $\dot{f}(Z_P)$. The optimal values of the parameters controlling the temperature polynomials are given in Table 2. Note that $dg_{so}(T_L)/dT$ is the slope of the linear soot oxidation temperature function. The comparison between prediction and experiment shown in Figs. 3–6 was performed using the parameters listed in Tables 1

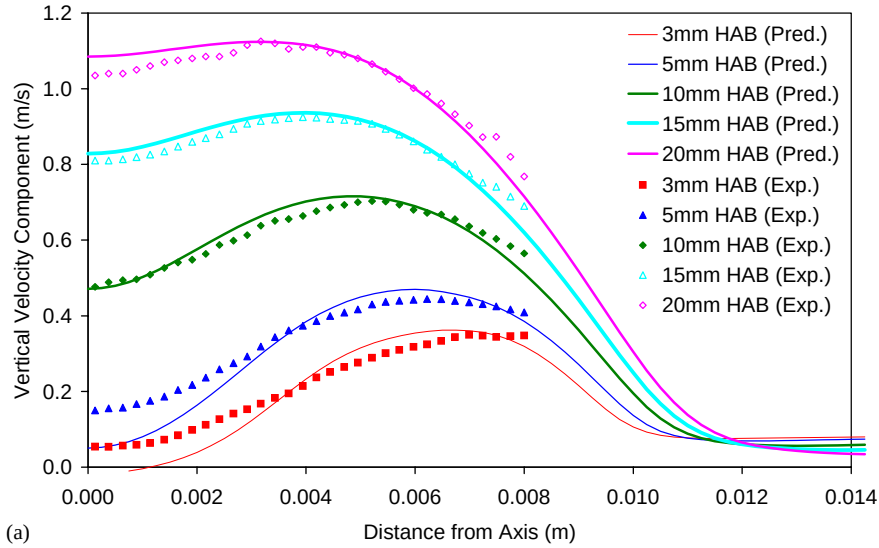

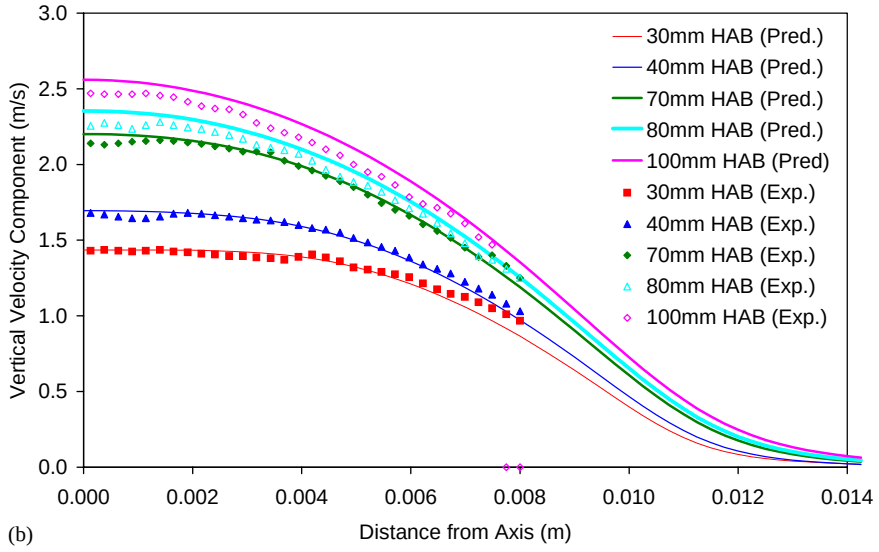

Fig. 5. Optimal vertical velocity predictions in 212 W ethylene flame at several heights above burner (HAB): (a) 3–20 mm, (b) 30–100 mm.

and 2. The analytic soot formation map generated using the parameters from Tables 1 and 2 is presented in Fig. 7. This is a graphical representation of the soot formation rate as a function of mixture fraction and temperature that was found to give the best predictions in the 212 W ethylene flame.

The values of the optimal parameters in Tables 1 and 2 were determined by a manual calibration exercise and should be considered initial approximations. The

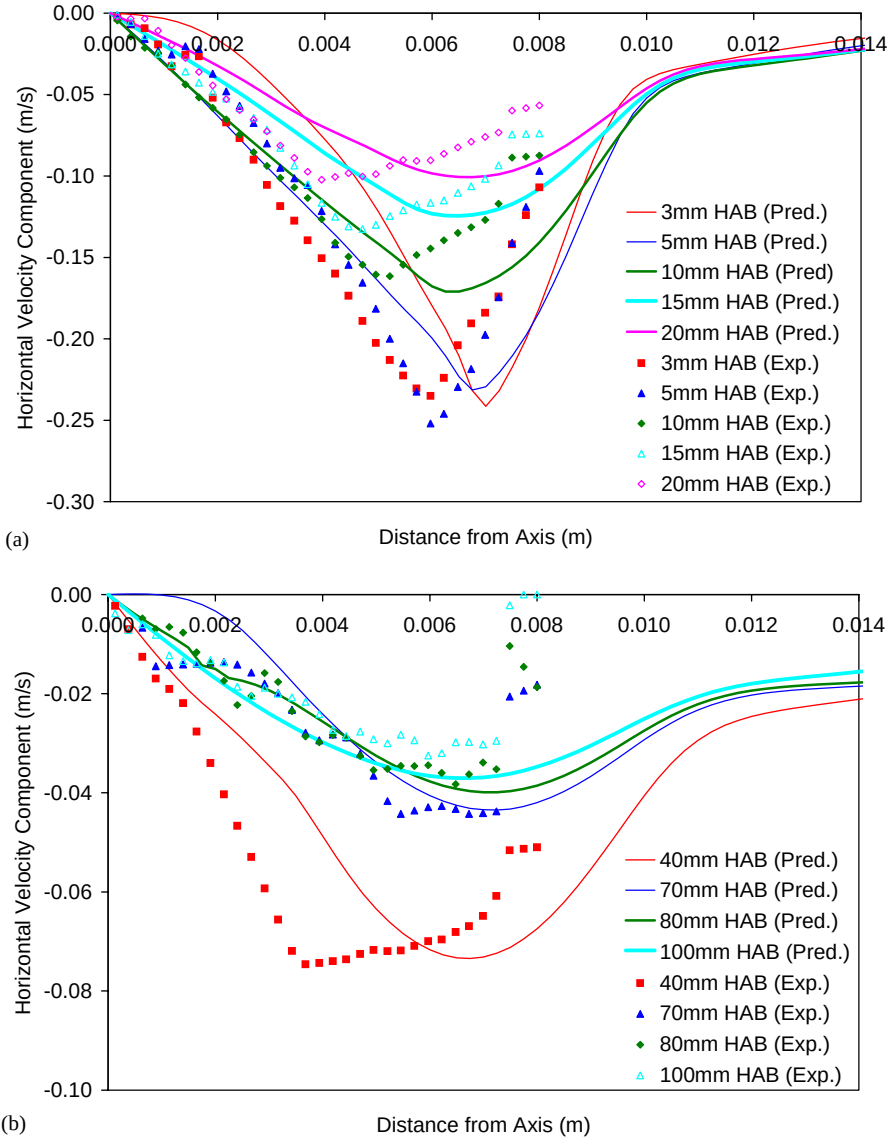

Fig. 6. Optimal horizontal velocity predictions in 212 W ethylene flame at several heights above burner (HAB): (a) 3–20 mm, (b) 40–100 mm.

calculations were made assuming a zero specific heat for soot and the heat liberated by the oxidation of unit mass of soot is equal to the heat liberated by the heat of formation of unit mass of CO_2. This approximation is presumably self-compensating for lightly sooting fuels but perhaps more severe for moderately to heavily sooting fuels.

Table 1
Optimal mixture fraction polynomial constants for 212 W ethylene flame

Parameter	Soot formation	Soot oxidation
ψ_{Z_L}	1.05	0.56
ψ_{Z_P}	1.77	0.84
ψ_{Z_H}	2.15	1.05
$\dot{f}(Z_P)$	1.10 kg/m^3 s	−0.85 kg/m^3 s

Table 2
Optimal temperature polynomial constants for 212 W ethylene flame

Parameter	Soot formation	Soot oxidation
T_L	1375 K	1375 K
T_P	1625 K	—
T_H	1825 K	—
$dg_{so}(T_L)/dT$	—	0.006 K^{-1}

6. Generalizing the model to other hydrocarbon fuels

The soot formation and oxidation model postulated herein contains thirteen adjustable constants (see Tables 1 and 2). Due to this large number of parameters, acceptable agreement between prediction and experiment can usually be achieved by adjusting different combinations of parameters. In general, the usefulness of a model decreases as the number of adjustable constants is increased [34]. However, a model retains its practicality if the constants are global, or if nonglobal constants can be estimated from simple rules or empirical material properties. This is the approach taken here: all constants listed in Tables 1 and 2, with the exception of the peak soot formation rate, are assumed fuel-independent. The inherent assumption is that the range of normalized mixture fraction over which soot formation occurs does not depend on the parent fuel. Although this approximation may not be capable of accurately reproducing detailed soot volume fraction profiles in laminar flames, it should be capable of capturing global trends. Keeping in mind that this model is intended for use in engineering calculations of radiation from fires, the ability to capture global trends is more important than the ability to reproduce detailed soot volume fraction profiles in small flames.

The smoke point flame mechanism provides the formula for the peak soot formation rate for a given fuel. The critical smoke point flame height for the release of soot occurs when the flow time, τ_{fs}, for fuel atoms traveling from the burner orifice to the flame tip equals the radiant cooling time, τ_{rs}. As the flow time increases, soot concentrations increase causing greater radiant heat loss and shortening the time for the flame to lose 30% of its heat and release unburned soot. The cooling time is the product of the radiant fraction, χ_{rs} and the heat content per unit volume of flame

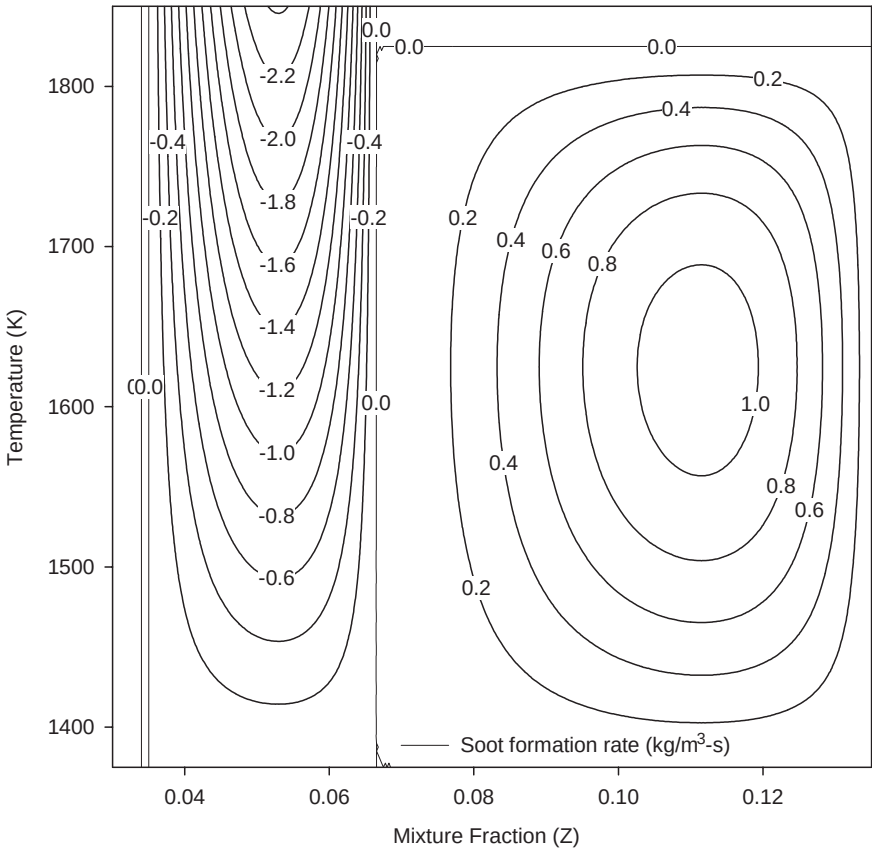

Fig. 7. Analytical soot formation map for 212 W ethylene flame.

gases, $(\Delta H_c/(S+1))\overline{\rho_f}$, divided by the mean radiant emission rate per unit volume of flame gases

$$\tau_{rs} \equiv \frac{\chi_{rs}(\Delta H_c/(S+1))\overline{\rho_f}}{\overline{\dot{q}'''_{rs}}}. \tag{22}$$

An overbar signifies an average over the entire flame; while the subscript "s" denotes the critical condition at the smoke point. The flow time for the buoyant flame is

$$\tau_{fs} \equiv \sqrt{\frac{2\ell_s}{g(\overline{\Delta\rho_f/\rho_f})}}. \tag{23}$$

The radiant emission from the soot can be calculated as

$$\overline{\dot{q}'''_{rs}} = 4(3.6)B_R\sigma\overline{T_{fs}^5}\,\overline{f_{vs}}/C_2. \tag{24}$$

Setting $\tau_{rs} = \tau_{fs}$ and eliminating $\overline{\dot{q}'''_{rs}}$ between Eqs. (22) and (24), and then substituting for τ_{fs}, one obtains the characteristic soot formation rate

$$\frac{Df_{vs}}{Dt} \cong \frac{\overline{f_{vs}}}{\tau_{fs}} = \frac{\chi_{rs}(\Delta H_c/(S+1))C_2}{4(3.6)B_r\sigma\overline{T_{fs}^5}}\left[\frac{\overline{\rho_f}g(\overline{\Delta\rho_f/\rho_f})}{2\ell_s}\right]. \tag{25}$$

The terms in square brackets are of primary interest. For hydrocarbon fuels burning in air, the terms in the front of the square brackets are insensitive to fuel type and depend almost exclusively on the adiabatic stoichiometric flame temperature. Specifically: (1) the radiant fraction at the smoke point, χ_{rs} depends only on the adiabatic stoichiometric flame temperature [5]; (2) the ratio $\Delta H_c/(S+1)$ is quite insensitive to fuel type for flames burning in air; (3) the temperatures, T_{fs} at homologous positions throughout flames at their smoke point are almost identical for hydrocarbons burning in air [10]; (4) the remaining terms in front of the square brackets do not depend on fuel type.

The ratio $\overline{\rho_f}/\ell_s$ inside the square brackets increases with the square of pressure. This comes from the facts that $\overline{\rho_f}$ is proportional to pressure while the smoke point height, ℓ_s, is inversely proportional to pressure for hydrocarbon flames burning in air [18]. There is a considerable literature supporting the soot formation rate being inversely proportional to the smoke point flame height of the fuel [7,9,11,15]. The remaining expressions in Eq. (25) are independent of pressure.

Eq. (25) does not suggest that the soot formation rate is proportional to the acceleration of gravity, g. This would be impossible. The molecules participating in the soot formation process cannot be directly affected by gravity but can only be affected by the local flame chemistry. Instead as gravity increases the flames must become taller to maintain them at the smoke point with flow time equal to the radiation cooling time.

Buoyancy of the flow $g\overline{\Delta\rho_f/\rho_f} = g\overline{(\rho_\infty - \rho_f)/\rho_f}$ probably depends on the molecular weight of the fuel—decreasing with increasing fuel molecular weight. The ambient density, ρ_∞, is independent of fuel molecular weight; whereas the fuel or flame density, ρ_f, increases with molecular weight. The exact dependence on molecular weight is not apparent from this formula; however, we presume here that the appropriate peak soot formation rate is inversely proportional to the fuel molecular weight.

The above analysis applies to pure hydrocarbons burning in air. It has been established [35,36] that soot formation rates are also linearly proportional to the mass fraction of fuel in the fuel supply stream, Y_{FT}. One finally arrives at the following expression for the peak soot formation rate:

$$\dot{\omega}'''_{sf,P} = 1.1\left(\frac{0.106}{\ell_s}\right)\left(\frac{28}{M_F}\right)^n\left(\frac{p_0}{p^\circ}\right)^2 Y_{FT}\ \mathrm{kg/m^3\ s}. \tag{26}$$

In Eq. (26), the peak soot formation rate is given as a function of the background pressure p_0 normalized by the reference pressure p° (101.3 kPa), the smoke point flame height for a pure fuel ℓ_s, and the fuel's molecular weight M_F. The proper numerical value of the exponent n in Eq. (26) is uncertain, but we use $n = 1$ in this

work. The constant in the first parenthetical term is the laminar smoke point height of ethylene (0.106 m) and the constant in the second set of parentheses is ethylene's molecular weight. The leading constant was selected so this expression matches the peak soot formation rate of the laminar 212 W atmospheric pure ethylene flame burning in air (1.1 kg/m^3 s) given in Table 1.

One can apply Eq. (26) to mixtures of hydrocarbon fuels by assuming linear superposition of hydrocarbons (and $n = 0$ in Eq. (26)) to obtain

$$\frac{1}{\ell_s} = \frac{1}{\overline{M}} \sum_i \frac{X_{Fi} M_{Fi}}{\ell_{si}} = \sum_i \frac{Y_{Fi}}{\ell_{si}}. \tag{27}$$

Gill and Olson [16], and Markstein [17] showed that the smoke point height of a fuel mixture follows the relation for both liquid and gaseous fuels. In Eq. (27), Y_{Fi} is the mass fraction of species i in the fuel stream and ℓ_{si} is the smoke point height for the respective pure fuel species.

7. Predictions using the generalized model

The generalized model was given a cursory test by comparing its predictions to the measured soot absorption cross-section per unit height α_s (m) in laminar ethylene, propylene, and propane flames [7,31]. The soot absorption cross-section per unit height is a measure of the total integrated amount of soot present at a given height in the flame and is a more global test of the soot model than the detailed profile comparisons shown above. Table 3 gives the experimental configurations of the flames included in the data sets [7,31], and Table 4 gives the smoke point data for ethylene, propylene, and propane. In Table 3, V_a is the air coflow velocity in millimeter per second, V_F is the fuel velocity in mm/s, and Q_F is the fuel flowrate in

Table 3
Experimental configurations of flames used for comparison of prediction and experiment

Fuel	Burner ID (mm)	V_a (mm/s)	V_F (mm/s)	Q_F (cm^3/s)	HRR (W)
Ethylene [7]	6	50	21.5	2.43	134
Ethylene [7]	6	50	32.3	3.65	201
Ethylene [7]	6	50	43.0	4.86	268
Ethylene [7]	6	50	53.8	6.08	335
Propylene [7]	6	50	5.1	0.58	46
Propylene [7]	6	50	7.7	0.87	69
Propylene [7]	6	50	10.3	1.17	93
Propylene [7]	6	50	12.9	1.46	117
Ethylene [31]	11	86.6	39.8	3.85	212
Ethylene [31]	11	86.6	41.4	4.00	220
Ethylene [31]	11	106	45.8	4.43	244
Ethylene [31]	11	106	47.6	4.60	253
Propane [31]	11	86.6	26.5	2.57	213

Table 4
Laminar smoke point data for ethylene, propylene, and propane

Fuel	Formula	ℓ_s (m)	$\dot{Q}_{sp}$ (W)
Ethylene	C_2H_4	0.106	212
Propylene	C_3H_6	0.029	69
Propane	C_3H_8	0.162	303

cubic centimeters per second. The corresponding heat release rate is listed in the rightmost column.

The first eight flames in Table 3 were investigated by Markstein and de Ris [7]. They are axisymmetric ethylene and propylene flames burning on a 6 mm ID fuel tube with a coflowing air stream. The soot absorption cross-section per unit height was measured via laser light extinction ($\lambda = 0.94\,\mu m$) as a function of height above the burner. The last five flames listed in Table 3 are from data compiled by Smyth [31]. The Smyth data sets included detailed soot volume fraction profiles. In order to allow for direct comparison with the Markstein and de Ris data [7], the soot absorption cross-section per unit height $\alpha_{s\lambda}$ was calculated from the detailed soot volume fraction profiles [31] at each height in the flame by evaluating the radial integral in Eq. (28)

$$\alpha_{s\lambda} = \int_0^\infty 2\pi r k_{s\lambda}\, dr. \tag{28}$$

The effective absorption coefficient $k_{s\lambda}$ is determined from the soot volume fraction profiles at the wavelength used to obtain the experimental data. Eq. (28) was also used to express the predicted soot volume-fraction-profiles in terms of the radially integrated soot absorption cross-section.

The significance of these experimental measurements [7,31], and the reason that they were chosen as a test of the present soot model, is that the experimental soot absorption cross-section per unit height profiles exhibit similarity when normalized by $\dot{Q}/\dot{Q}_{sp}$ and plotted as a function of the flame height normalized by the smoke point height. The measured soot absorption cross-section profiles fall on the same curve when plotted after being normalized in this manner. This is true below values of $H/\ell_f \approx 0.6$ where H is the height above the burner and ℓ_f is the flame height ($\ell_f = \ell_s \dot{Q}/\dot{Q}_{sp}$). Differences at greater values of H/ℓ_f are attributed to the transition from a nonsmoking to a smoking flame.

A comparison between the predicted and measured soot absorption cross-section per unit height for the Markstein and de Ris flames [7] is shown in Figs. 8 (ethylene) and 9 (propylene). Similarly, the comparison between prediction and experiment for the Smyth flames [31] is given in Figs. 10 (ethylene) and 11 (propane).

It can be seen from data shown in Figs. 8 and 9 that the peak magnitude of the soot absorption cross-section is predicted relatively well, and the predicted profiles exhibit the same similarity that is observed experimentally. However, the predicted profiles peak at lower values of H/ℓ_f than the experimental profiles. The peak of the

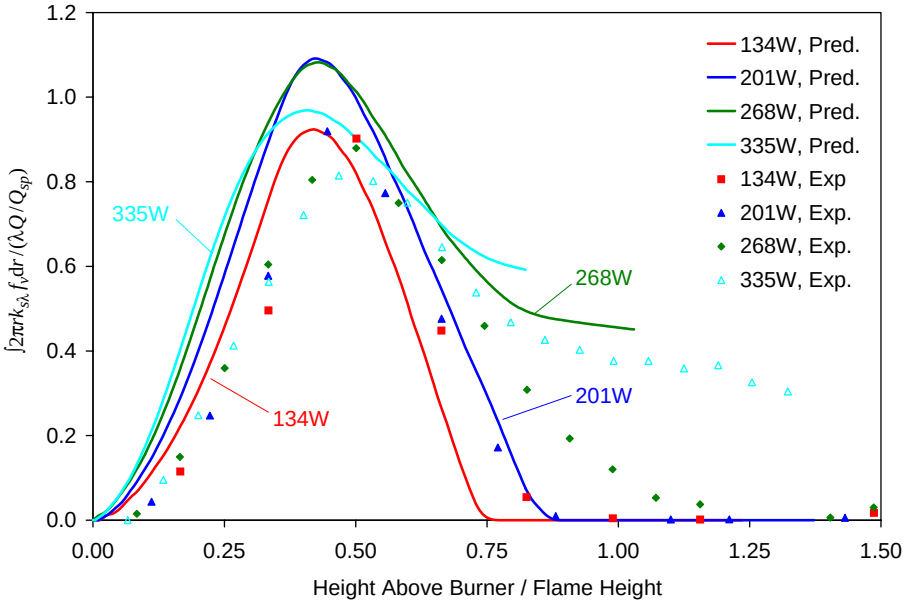

Fig. 8. Ethylene absorption cross-section per unit height from Markstein and de Ris data.

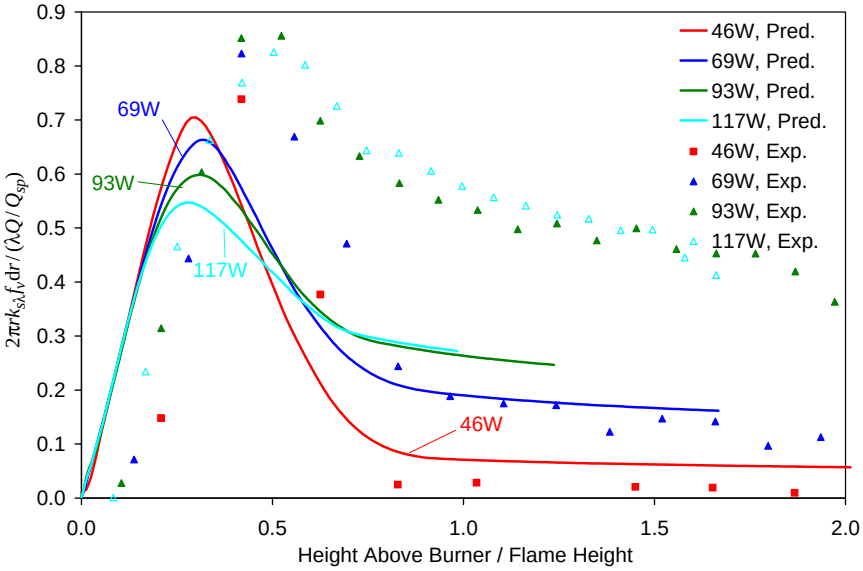

Fig. 9. Propylene absorption cross-section per unit height from Markstein and de Ris data.

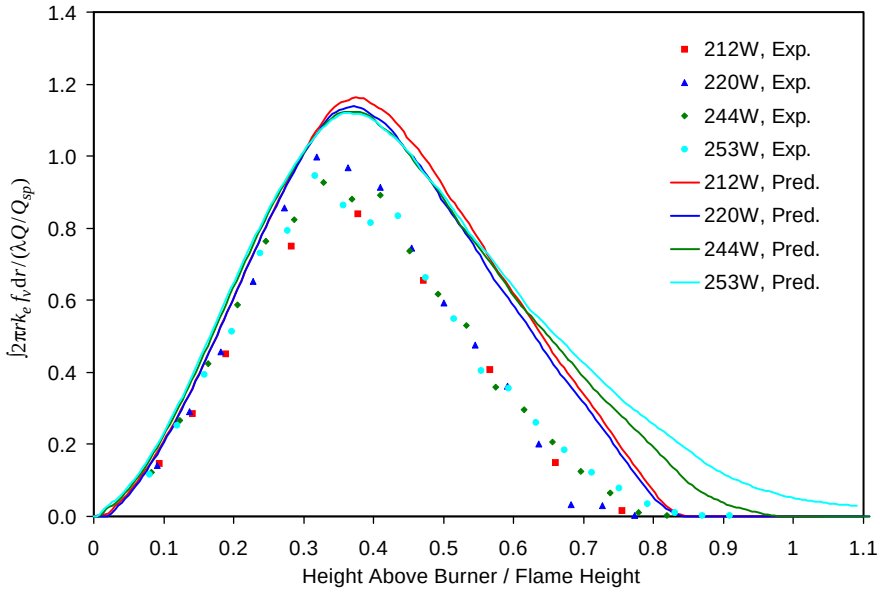

Fig. 10. Ethylene absorption cross-section per unit height from Smyth data.

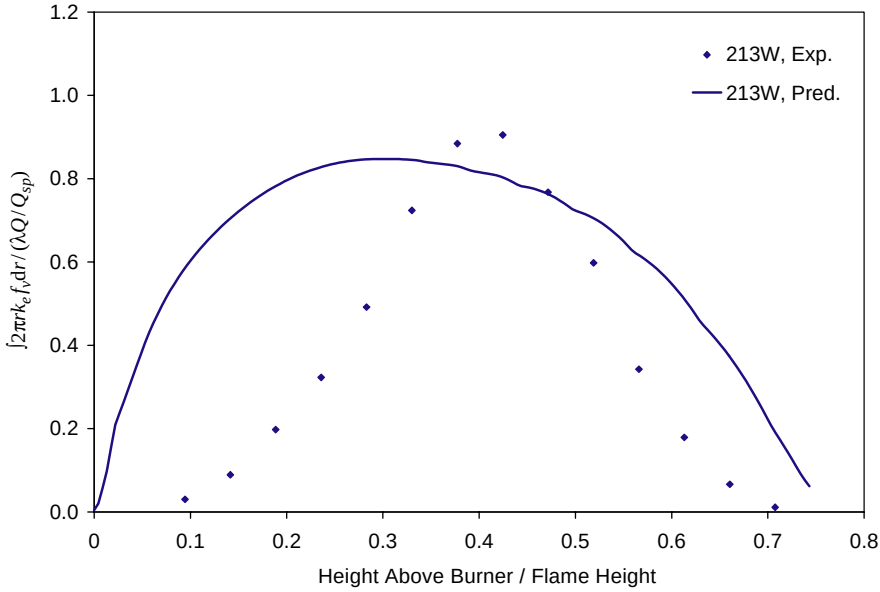

Fig. 11. Propane absorption cross-section per unit height from Smyth data.

soot cross-section profiles corresponds to the transition from soot formation to oxidation, which occurs at mixture fraction values close to stoichiometric. Since the mixture fraction conservation equation contains a source term of opposite sign to the soot formation/oxidation source term, soot formation corresponds to a sink of mixture fraction and "pushes" the mixture fraction closer to its stoichiometric value. In flames where soot formation is overpredicted, the mixture fraction will approach its stoichiometric value more quickly than it should. This causes the transition from soot growth to soot oxidation to occur lower in the flame, explaining why the peak of the soot profile occurs at a lower value of H/ℓ_f than seen experimentally. This highlights the highly coupled nature of the processes being modeled here.

Figs. 10 and 11 show a comparison of prediction and experiment in the ethylene and propane flames reported by Smyth [31]. These flames were established on a fuel tube with an ID of 11 mm, whereas the Markstein and de Ris flames [7] used a burner with an ID of 6 mm. The predicted and measured ethylene data show a high degree of similarity when scaled by the smoke point heat release rate, consistent with our hypothesis that the smoke point is the controlling parameter for soot formation. In the ethylene flames, the predicted and measured amounts of soot match quite well low in the flame. This is to be expected because the soot model parameters were calibrated for the 212 W ethylene flame [31] on this 11 mm ID burner. The transition from soot formation to oxidation does not occur as quickly in the simulations as in the experiments, indicating that the soot oxidation component of the model needs adjustment.

Comparison of prediction and experiment for the propane flame, which is lightly sooting and has a smoke point of 16.2 cm, shows that the model predicts that far too much soot is formed low in the flame. This is expected because surface area-dependent soot formation is increasingly important in lightly sooting flames. The model used here does not consider heterogeneous soot formation and contains no mechanism to suppress homogeneous soot formation at short residence times. These results indicate that the model should not be used without modification for flames less sooty than ethylene, i.e., fuels with a smoke point height greater than ~11 cm. This includes several of the lower molecular weight normal alkanes such as methane, ethane, propane, butane, pentane, and heptane. However, the model should apply to the majority of all normal alkanes, substituted alkanes, cyclic alkanes, normal alkenes and polyolefins, cyclic alkenes, dienes, normal alkynes, and aromatics as most have smoke point heights less than 11 cm (see Appendix K of Lautenberger [22]).

8. Concluding remarks

A new framework intended for engineering calculations of soot formation/oxidation and flame radiation from non-premixed flames of hydrocarbon fuels has been developed and subjected to an initial calibration. The basic approach, though promising, is not yet mature. The purpose of disseminating this research in its current state is to encourage others to enhance and simplify the model, make use of

the ideas contained in this paper, and proceed forward in an area for which there is currently no entirely tractable solution for engineering calculations.

Conceptually the model is rather simple. Soot and gas are described as separate phases. The local state of gas within the flame is expressed in terms of two canonical variables, (1) the mixture fraction and (2) the chemical enthalpy that reflects the effect of any prior energy loss (gain) by radiation. The reactant stoichiometry and smoke point are model parameters. The model conforms to the large body of data in the literature showing that the fuel smoke point correlates the release of radiation, smoke and CO from turbulent non-premixed flames.

Simplicity is achieved by the recognition that soot oxidation in non-premixed flames is controlled by the diffusion of oxygen into the zone of active soot oxidation rather than being limited by reaction of $OH\cdot$ radicals impinging on the available soot surface area. This control by diffusion explains: (1) the observed near perfect similarity of soot distributions in laminar smoke point flames for different fuels, as well as, (2) the dependence of soot formation and oxidation on the Kolmogorov microscale in turbulent non-premixed flames.

The rate of soot formation of a fuel is inferred directly from an understanding of the smoke point mechanism. Other than the smoke point, the model uses fuel-independent properties, making it easy to apply to different fuels including fuel mixtures. In contrast to most earlier empirical models of soot formation, the model presented here considers only homogeneous (surface area-independent) soot formation, thereby eliminating the need to solve a conservation equation for the soot number density and minimizing computational cost. It is likely that surface area-dependent soot formation is important in lightly sooting fuels, but becomes less important for heavily sooting fuels. This model is therefore appropriate for use with sooty fuels, which are often of interest in fire safety engineering due to their increased radiative transfer.

An initial calibration exercise in a small-scale laminar ethylene flame was used to establish global values for the model parameters. A test of the model's applicability to other fuels was performed by using the global model parameters to examine the radially integrated amount of soot as a function of height above the burner in ethylene, propylene, and propane candle flames at several fuel flow rates [7,31]. The results, though encouraging, indicate that future work is required.

9. Suggestions for future work

Due to the drastic simplifications and approximations made here, we encourage future theoretical, experimental, and numerical work to guide refinement of these assumptions. In particular, computations using the temperature-dependent soot reaction enthalpies given in Eq. (10) could be used in lieu of the fixed values actually employed here to determine if such a simplification is reasonable. Additional experimental measurements in diffusion flames would be useful, because the model parameters have physical significance and could potentially be measured for different fuels. For example, the soot inception temperature, the maximum

temperature above which soot no longer forms, and the range of stoichiometry over which soot forms are all required model input parameters that could be measured experimentally for different fuels and compared to the values suggested in this work. These measurements could then confirm or refute the hypothesis that soot formation region given by the normalized mixture fraction is invariant from fuel to fuel.

Theoretical work, used as a complement to experimental measurements, also has the potential to help improve this model. The "blue zone" at the base of lightly sooting non-premixed flames cannot be captured by this model in its present form. In this region, soot formation is initially delayed and likely subject to surface area control, so the rate of appearance of soot precursors must be considered. Additionally, theory suggests that the soot oxidation rate is restricted by the Arrhenius expression for the decomposition of O_2 by the radical $H\cdot$, but linear dependence is used here for simplicity. It may be possible to show that an Arrhenius temperature dependency is superior and should be used. The volumetric (soot surface area-independent) oxidation rate proposed here could be investigated with a combined experimental, theoretical, and numerical study.

Acknowledgements

The authors wish to express their appreciation to FM Global Research and Dr. Robert G. Bill who patiently encouraged this research. We would also like to thank Dr. Kevin B. McGrattan at NIST for his insightful comments and making the FDS code practical.

Appendix. Review of soot formation and oxidation

The main paper presents a smoke point-based model of soot formation and oxidation in non-premixed flames. It provides a new approach to a subject having a long history and extensive literature. In Appendix A, we review some of this literature, discuss some difficulties, and justify the need for a new approach to this important subject.

Much of the knowledge of the chemistry of soot formation and oxidation comes from measurements made on premixed flames. Premixed flames have relatively rapid gas-phase reaction rates due to their large concentrations of free radicals. In the presence of these fast gas-phase reactions, the rate-limiting steps for soot formation and oxidation typically include the mass transfer processes between solid and gas-phases such as particle nucleation, surface growth and oxidation. In such circumstances, the available soot surface area limits the formation and destruction of soot and becomes an integral part of the mechanism controlling soot formation and oxidation.

In contrast, soot formation in non-premixed flames is usually controlled by gas-phase processes. In non-premixed flames, reactions are limited primarily by diffusion of gaseous reactants to the flame sheet. The main heat releasing reactions occur in a

thin sheet comprising a narrow range of mixture fraction. Elsewhere in the flame, gas-phase reaction rates are slowed by the presence of hydrocarbons that tend to scavenge H· atoms and other free radicals. This picture is consistent with the observation of almost "frozen" conditions occurring on the fuel-rich side of hydrocarbon diffusion flames. In this frozen zone, the concentrations of species are primarily determined by the nature of the supplied reactants and the local mixture fraction while being insensitive to the overall heat release rate of the flame. This simplifies the description of the chemical environment for the formation of soot in regions separated from the main reaction zone, i.e., in regions where the chemical and thermal environments are determined by the local mixture fraction and enthalpy (temperature). It is therefore not surprising that the spatial distributions of the soot volume fraction in non-premixed flames exhibit similarity when scaled by only the smoke point of the fuel [7–10]. The more traditional view thinks of soot formation as being controlled by surface reactions wherein soot particles are nucleated in the main heat-release reaction-zone and then move by convection and thermophoresis into fuel-rich zone where most of the soot growth occurs by surface reactions.

Viewed from the above perspective, one anticipates soot formation in non-premixed flames being gas-phase controlled on the fuel-rich side in the presence of significant hydrocarbons, and surface area controlled in the narrow heat-release reaction-zone where the concentrations of free radicals are high. The relative importance of these two mechanisms depends on the particular fuel and oxidant. For moderate to sooty fuels, the subject of the main paper, soot forms predominately in the hydrocarbon-rich zone. Methane, being quite chemically stable and lightly sooting, is at the other extreme. It does not even have a meaningful smoke point. Soot in methane flames forms largely in the high temperature "wings" and is presumably surface area controlled. As a general trend, for most fuels, soot tends to form increasingly in the wings as one increases the ambient oxygen concentration, whereas in oxygen depleted atmospheres, soot tends to form predominately in the hydrocarbon-rich core.

The model presented in the main paper postulates soot forming immediately upon the mixture fraction falling within its soot formation range provided the temperature is within the soot formation range. As such, it does not account for the finite time it takes for the fuel molecules to break apart, form aromatic rings, and then nucleate particles. One observes this delay by the presence of a blue zone at the base of the flame. Methane has a particularly large blue zone at base of its flame, but the blue zone is much less prominent for sooty fuels.

In a similar manner, a finite time is required for soot to form in the hydrocarbon rich zone. Upon insertion of a probe into this zone, one observes the thermophoretic deposition onto the probe of a brown liquid that under a microscope appears spaghetti-like. Unlike soot, the brown condensate in the flame is transparent to laser light. Subsequently, as the liquid carbonizes to form soot, it becomes visible to laser light. Dobbins [37] quantified the phenomenon for an ethylene flame.

From the above discussion, it is apparent that soot formation occurs by a variety of detailed chemical mechanisms. The possibility of competing chemical mechanisms complicates the situation. Frenklach [38] reviews much of the recent literature on the

chemistry of soot formation. He emphasizes that to establish detailed chemical models of the evolution of soot one must accurately describe both the chemical and thermal gas-phase environment.

In view of such complexities, it helps to recall that from an engineering viewpoint, it is the release of radiant heat, smoke, and products of incomplete combustion that is most important. These releases are all well correlated by the fuel smoke point, which in turn is quite simply explained by the model presented in the main paper. The model, while approximate, captures the essential chemistry and physics needed for engineering applications.

A.1. Traditional modeling approaches

Several models for soot formation in non-premixed flames already exist, and Kennedy [39] has provided an excellent review of work before 1997. These models rely on empirical data. Some models make direct use of experimentally measured or inferred quantities [23,27]. Other models indirectly use experimental measurements for calibration, where model parameters are adjusted until agreement between prediction and experiment is obtained [25]. These models do not have a set of "rules" that explains how to determine the model constants for an arbitrary fuel. One shortcoming of this type of approach is that these models are usually appropriate for use only with a specific fuel, oxidant, pressure, and combustor. Extension of a model beyond the operating conditions for which it was developed may lead to unreliable predictions. Therefore, this type of model is impractical for use in fire safety engineering where a variety of fuels is encountered.

Most empirical soot models contain expressions to quantify a limited number phenomena usually considered important for soot formation and oxidation. As pointed out by Lindstedt [40–42], it is generally agreed among traditional modelers that a simplified model of particulate formation in diffusion flames should account for the processes of nucleation/inception, surface growth, coagulation/agglomeration, and oxidation. For this reason, most models explicitly consider these processes. This paradigm is based on the classical view of soot formation in diffusion flames where incipient soot particles with diameters on the order of several nanometers form in slightly fuel-rich regions of the flame by inception or nucleation. These particles then undergo surface growth, perhaps by the Hydrogen Abstraction by C_2H_2 Addition (HACA) mechanism [43], with $H\cdot$ atoms impacting on the soot surface to activate acetylene addition, thereby increasing the mass of existing soot particles. Since HACA is initiated by $H\cdot$ atoms, it is likely to be most important in the main flame reaction zone where $H\cdot$ atom concentrations generally exceed equilibrium values. As discussed in the main paper, there is an alternative route to soot through Polycyclic Aromatic Hydrocarbons (PAHs), which becomes important in hydrocarbon-rich regions (away from the main reaction zone) where the $H\cdot$ atom concentrations are low. This soot growth occurs concurrently with coagulation, where small particles coalesce to form larger primary particles, and agglomeration where multiple primary particles line up end-to-end to form larger structures resembling a string of pearls. Soot particles may be transported toward the flame

front where they pass through an oxidation region in which the mass of soot is decreased by oxidation reactions with gas-phase molecules. Any soot not completely oxidized is released from the flame envelope as "smoke" [44].

Most traditional models of soot formation and oxidation provide a means to quantify each of the phenomena outlined above. They are embedded within a CFD model that provides the necessary flowfield quantities such as species concentrations, temperature, and velocity. Typically, conservation equations are solved for the soot mass fraction Y_s (or the soot volume-fraction, f_v) and the soot number density, N. The soot conservation equation contains separate terms to account for the increase in f_v attributed to either particle inception/nucleation or surface growth. Conversely, a term is included to account for the sink of f_v ascribed to soot particle oxidation. Models that explicitly consider particle inception/nucleation and coagulation/agglomeration must also solve a conservation equation for the number density that includes a source representing particle inception, and a sink representing particle coagulation/agglomeration. The rates of particle inception, coagulation, agglomeration, surface growth, and oxidation are then quantified through the postulated expressions that constitute the soot model.

Reilly et al. [45,46], citing their experimental findings in acetylene diffusion flames using Real-Time Aerosol Mass Spectrometry, have questioned whether the above classical view of soot formation embodied in these models is representative of the actual physical and chemical phenomena of soot formation in non-premixed flames. It is fair to ask whether a successful soot model, particularly one intended for engineering calculations, must include expressions for each of the components identified above. Lindstedt [42] showed that his predictions of soot volume fraction in three counterflow ethylene flames were relatively insensitive to the particular form of the nucleation model used after fitting the models to data. This casts doubt on whether the nucleation is part of the controlling mechanism of soot formation in non-premixed flames. Additional problems with this classical view are presented below.

A.2. Physical and chemical factors affecting soot formation

The specific soot area is important if heterogeneous surface reaction between soot particles and the gas-phase is the dominant mechanism for soot growth. If this was the case, one would expect the rate of soot addition to be proportional to the soot surface area available for growth. To account for the observed decrease in proportionality to the specific soot surface area (m^2 soot/m^3 mixture), scientists have introduced the concept of soot aging. The dependence of soot formation rates on a particle's history is explained by the notion that as a soot particle ages, the number of active sites on its surface capable of supporting chemical reactions may change due to annealing. It would have been simpler, instead, to have attributed the observed decrease in reactivity to control by gas-phase processes.

Bonczyk [47] investigated the effect of ionic additives on particulate formation in non-premixed flames. His results showed an order of magnitude increase in the soot number density with only a slight increase in the soot volume fraction, indicating the

available soot surface area is not part of the controlling mechanism in the flames studied. Delichatsios [48], relying heavily on experimental observations, has also postulated that homogeneous gas-phase reactions and not heterogeneous surface growth reactions are the controlling mechanisms of soot formation in diffusion flames. He showed that the results of several experimental studies could not be readily explained if the rate of soot formation is dependent on the specific soot surface area.

It is likely that both surface area-dependent and surface area-independent mechanisms contribute to the overall rate of soot formation in diffusion flames. As part of the present work, we investigated a model that considered surface area-dependent, surface area-independent, or both mechanisms of soot formation. When using only surface growth, the "wings" (soot that forms low in the flames far from its axis) could be reproduced reasonably well, but the soot loading at the "core" (near the flame axis) was underpredicted for ethylene flames. This is consistent with the study of Liu et al. [26] where it is noted that soot formation models based on surface area-dependent growth by acetylene addition underpredict the soot loading along the flame axis. Similarly, we found that when using only a volumetric growth mechanism, the soot loading at the core of methane flames could be reproduced, but far too much soot was predicted in the wings. We found that the additional adjustable constants in a soot formation model that considered both mechanisms could reproduce the soot volume-fraction profiles reported by Smyth [31] for axisymmetric methane, propane, and ethylene flames reasonably well. However, with competing soot formation mechanisms, the conceptual simplicity of having the soot formation rate being dependent only on the fuel smoke point flame height was lost. This conceptual simplicity is supported by the analytical arguments of Section 6 and the literature [7,9,15,19,49]. For this reason, we chose a model that contains only a volumetric growth mechanism. The presumption here is that homogeneous processes are the dominant soot formation mechanism for moderately to heavily sooting fuels.

In summary, the above arguments have led to the surmise that the abundance of $H\cdot$ radicals near the outer wings of the diffusion flame cause the soot to form there by the HACA mechanism [43] subject to surface area control. In the core regions, where negligible $H\cdot$ atoms are present, soot generation takes place primarily through the formation of PAHs subject largely to gas-phase control. Hwang and Chung [50] reached a similar conclusion through an experimental and computational study of ethylene counterflow diffusion-flames that was conducted to examine the relative importance of acetylene and PAHs in soot growth. They reported that satisfactory agreement between predicted and measured soot mass growth rates could be obtained if two separate pathways to soot formation were considered. They concluded that the HACA mechanism is the dominant mode of soot formation in the high temperature regions, but coagulation between PAH and soot particles is quantitatively important in the low temperature regions. The latter may account for up to 40% of the contribution to soot formation in these counterflow flames [50].

This basic hypothesis is also supported by the experimental study of Zelepouga et al. [51] in which laminar co-flow methane flames were doped with acetylene and PAHs. For the flame burning in a 21–79% mixture of O_2–N_2, the peak soot

concentrations were increased by approximately 40–75% when the flames are seeded with 1.0 carbon percent (C%) pyrene (a PAH), but only by 15–50% when seeded with 3.7C% acetylene. The seeding levels are reported in C% to account for the different C:H ratios of the various additives. A larger increase in soot volume fraction was induced by doping the flame with acetylene than with pyrene low in the flame near the high-temperature reaction sheet. However, the pyrene induces a much larger increase in soot volume fraction compared to acetylene at greater distances from the reaction zone and near the core. This indicates that different soot formation mechanisms are dominant in different regions of this flame.

Zelepouga et al. [51] also made measurements for different amounts of additives to methane non-premixed flames in different ambient oxygen atmospheres. In the case of added acetylene, the fractional increase in soot was proportional to the added acetylene with proportionality remaining the same with increased ambient oxygen. In the case of pyrene, the fractional increase in soot was also proportional to the added pyrene, but the proportionality constant increases strongly with increased ambient oxygen concentration. The acetylene result implies that the path for soot formation in methane flames always goes through acetylene for methane burning in air or oxygen-enriched air, whereas the pyrene result indicates the role of PAHs differs in different regions of the flame having different sensitivity to ambient oxygen. Near the flame sheet, the HACA mechanism [43] (dependent on the available surface area) may be controlling; yet near the core, a mechanism involving growth by PAHs that is independent of surface area becomes significant. It is worth pointing out that Zelepouga et al. [51] investigated only lightly sooting *methane* flames and that the relative importance of the PAH route increases for sootier fuels.

A.3. Factors affecting soot oxidation

Soot oxidation is usually modeled as a heterogeneous process where the oxidation rate is proportional to the available soot surface area. Several species have been linked to soot oxidation in hydrocarbon diffusion flames, most notably $OH\cdot$, O_2, and $O\cdot$. There has been a considerable debate over the relative importance of these oxidizing species. Neoh et al. [28] clearly demonstrated the importance of soot oxidation by $OH\cdot$ radical, particularly on the fuel side of stoichiometric. They concluded that under the conditions studied, $OH\cdot$ was the principal oxidant, with molecular oxygen becoming important only for O_2 concentrations above 5%. The $H\cdot$ radical usually occurs in low concentrations so it is of less concern here. These results have recently been confirmed for diffusion flames [52].

Puri et al. [29,30] experimentally studied the oxidation of soot and carbon monoxide in laminar axisymmetric methane, methane/butane and methane/1-butene diffusion flames. They measured $OH\cdot$ radical as well as the CO and soot concentration profiles at several axial positions and found that the $OH\cdot$ concentrations are far higher than their equilibrium values wherever hydrocarbons have been consumed. In general, $OH\cdot$ reacts more readily with CO than with soot. This explains why CO tends to be consumed first. The presence of soot, however, significantly depresses $OH\cdot$ concentrations in soot-laden regions. Molecular oxygen

concentrations remain very small in regions of active soot oxidation. This is important from a modeling perspective. It means that the generation of $OH\cdot$ and therefore the consumption of CO and soot are controlled by the diffusion of O_2 into the soot oxidation zone rather than being controlled by the surface area of soot. This suggests that the rate of soot oxidation is a function of the mixture fraction. When the radiant heat loss from the soot cools the flame below approximately 1400 K, the generation of $OH\cdot$ decreases and soot oxidation slows to the point of releasing soot. Once the soot leaves the active flaming region, its oxidation is likely to be surface area controlled.

One may gain further understanding of soot oxidation process by considering the following simplified soot oxidation reaction mechanism:

$$C_{soot} + OH\cdot \rightarrow CO + H\cdot \tag{A.1a}$$

$$CO + OH\cdot \rightarrow CO_2 + H\cdot \tag{A.1b}$$

$$O2 + H\cdot \rightarrow OH\cdot + O\cdot \tag{A.1c}$$

$$O\cdot + H_2O \rightarrow OH\cdot + OH\cdot \tag{A.1d}$$

$$H\cdot + OH\cdot + (M) \rightarrow H_2O + (M) \tag{A.1e}$$

The above reactions collectively sum to:

$$C_{soot} + O_2 \rightarrow CO_2. \tag{A.2}$$

The first four reactions (Eqs. (A.1a–A.1d)), being bimolecular, are relatively fast for temperatures above 1400 K. However, Eq. (A.1e) is a three-body recombination reaction that is quite slow because it requires the simultaneous collision of three molecules. Its slowness leads to a build-up of $H\cdot$ and $OH\cdot$ radicals far above their equilibrium values. The super-equilibrium concentration of radicals leads to the immediate consumption of any molecular oxygen that manages to diffuse to the reaction zone. When the temperature decreases below 1400 K, the recombination reaction 1e continues, while reaction (A.1c) between O_2 and $H\cdot$ slows to become the rate-limiting reaction for the entire mechanism. In such circumstances, the concentration of molecular oxygen builds up. Meanwhile, fewer radicals are generated and the soot and CO oxidation reactions, (A.1a) and (A.1b), slow down leading to the possible release of any soot or CO that had not been previously oxidized.

The above mechanism of soot oxidation in diffusion flames can be modeled by a volumetric soot oxidation rate that depends principally on the gas-phase composition with its maximum near stoichiometric. The temperature-dependence should be roughly proportional to the rate controlling reaction (A.1c), $O_2 + H\cdot \rightarrow OH\cdot + O\cdot$. This will allow for the release of soot under conditions of strong radiant cooling. The experimentally observed [7,10-11] similarity of axisymmetric diffusion flames at their smoke points corroborates the claim here that soot oxidation is controlled by the diffusion of molecular oxygen rather than the surface area of soot.

If the surface area were controlling, the observed similarity would never be achieved for the wide range of tested fuel smoke points.

References

[1] McGrattan KB, Baum HR, Rehm RG, Hamins A, Forney GP, Floyd JE, Hostikka S. Fire Dynamics Simulator (Version 2)—Technical Reference Guide, National Institute of Standards and Technology, NISTIR, 6783, 2001.
[2] McGrattan KB, Forney GP, Floyd JE. Fire Dynamics Simulator (Version 2)—User's Guide, National Institute of Standards and Technology, NISTIR, 6784, 2001.
[3] Zel'dovitch YB. Zhur Tekhn Fiz 1949;19:1199 English Translation, NACA Tech. Memo, No. 1296 (1950).
[4] Bilger RW. Reaction rates in diffusion flames. Combust Flame 1977;30:277–84.
[5] Markstein GH. Radiant emission and smoke points for laminar diffusion flames of fuel mixtures. Proc Combust Inst 1986;21:1107–14.
[6] ASTM. Standard Test Method for Smoke point of Aviation Fuels. Designation D1322-75 (Reapproved 1980).
[7] Markstein GH, de Ris J. Radiant emission and absorption by laminar ethylene and propylene diffusion flames. Proc Combust Inst 1984;20:1637–46.
[8] Olson DB, Pickens JC, Gill RJ. The effects of molecular structure on soot formation II. Diffusion flames. Combust Flame 1985;62:43–60.
[9] Kent JH. A quantitative relationship between soot yield and smoke point measurements. Combust Flame 1986;63:349–58.
[10] Gülder ÖL. Influence of hydrocarbon fuel structural constitution and flame temperature on soot formation in laminar diffusion flames. Combust Flame 1989;78:179–94.
[11] Kent JH. Turbulent diffusion flame sooting-relationship to smoke-point tests. Combust Flame 1987;67:223–33.
[12] Markstein GH. Measurements on gaseous-fuel pool fires with a fiber-optic absorption probe. Combust Sci Tech 1984;39:215–33.
[13] Markstein GH. Relationship between smoke point and radiant emission from buoyant turbulent and laminar diffusion flames. Proc Combust Inst 1984;20:1055–61.
[14] Tewarson A. Smoke point height and fire properties of materials. FMRC Technical Report No. J.I.0K3R3.RC, Factory Mutual Research Corporation, Norwood, MA, 1988.
[15] Delichatsios MA. Smoke yields from turbulent buoyant jet flames. Fire Safety J 1993;20:299–311.
[16] Gill RJ, Olson DB. Estimation of soot thresholds for fuel mixtures. Combust Sci Tech 1984;40:307–15.
[17] Markstein GH. Correlations for smoke points and radiant emission of laminar hydrocarbon diffusion flames. Proc Combust Inst 1988;22:363–70.
[18] Schalla RL, Clark TP, McDonald GE. Formation and combustion of smoke in laminar flames, NACA 1186, 1954.
[19] de Ris J, Wu PK, Heskestad G. Radiation fire modeling. Proc Combust Inst 2000;28:2751–9.
[20] Orloff L, de Ris J, Delichatsios MA. Radiation from buoyant turbulent diffusion flames. Combust Sci Tech 1992;84:177–86.
[21] Tewarson A. Generation of heat and chemical compounds in fires. In: SFPE handbook of fire protection engineering, 2nd ed. Quincy, MA: National Fire Protection Association, 1995, p. 396–8.
[22] Lautenberger CW. CFD simulation of soot formation and flame radiation. MS Thesis. Worcester, MA: Worcester Polytechnic Institute Center for Firesafety Studies; 2002. (Available online at http://www.wpi.edu/Pubs/ETD/Available/etd-0115102-002543/unrestricted/lautenberger.pdf.
[23] Kent JH, Honnery DR. Soot mass growth in laminar diffusion flames—parametric modelling. In: Bockhorn H, editor. Soot formation in combustion mechanisms and models. Berlin: Springer; 1994. p. 199–220.

[24] de Ris J, Cheng F. The role of smoke-point in material flammability testing. Fire safety science—Proceedings of the fourth international symposium, 1994. p. 301–12.
[25] Moss JB, Stewart CD. Flamelet-based smoke properties for the field modelling of fires. Fire Safety J 1998;30:229–50.
[26] Liu F, Guo H, Smallwood GJ, Gülder ÖL. Numerical modelling of soot formation and oxidation in laminar coflow non-smoking and smoking ethylene diffusion flames. Combust Theory Modelling 2003;7:301–15.
[27] Kent JH, Honnery DR. A soot formation rate map for a laminar ethylene diffusion flame. Combust Flame 1990;79:287–98.
[28] Neoh KG, Howard JB, Sarofim AF. Soot oxidation in flames. In: Siegla DC, Smith GW, editors. Particulate carbon formation during combustion, 1981. p. 261–77.
[29] Puri R, Santoro RJ, Smyth KC. The oxidation of soot and carbon monoxide in hydrocarbon diffusion flames. Combust Flame 1994;97:125–44.
[30] Puri R, Santoro RJ, Smyth KC. Erratum—the oxidation of soot and carbon monoxide in hydrocarbon diffusion flames. Combust Flame 1995;102:226–8.
[31] Smyth KC. Diffusion flame measurements of species concentrations, soot concentrations, temperature, and velocity. 1999. (Available online at http://www.fire.nist.gov/fire/flamedata/)
[32] Grosshandler WL. RADCAL: a narrow-band model for radiation calculations in a combustion environment. National Institute of Standards and Technology, NIST Technical Note 1402, 1993.
[33] Tien CL, Lee KY, Stretton AJ. Radiation Heat Transfer. In: SFPE handbook of fire protection engineering, 2nd ed. Quincy, MA: National Fire Protection Association; 1995.
[34] Lantz RV. Model validation in fire protection engineering. Ph.D. Thesis, Worcester, MA: Worcester Polytechnic Institute Center for Firesafety Studies; 2001. (Available online at http://www.wpi.edu/Pubs/ETD/browse/by_department/f.html).
[35] Axelbaum RL, Flower WL, Law CK. Dilution and temperature effects of inert addition on soot formation in counterflow diffusion flames. Combust Sci Tech 1988;61:51–73.
[36] Axelbaum RL, Law CK. Soot formation and inert addition in diffusion flames. Proc Combust Inst 1990;23:1517–23.
[37] Dobbins RA. Soot inception temperature and the carbonization rate of precursor particles. Combust Flame 2002;130:204–14.
[38] Frenklach M. Reaction mechanism of soot formation in flames. Phys Chem Chem Phys 2002;4:2028–37.
[39] Kennedy IM. Models of soot formation and oxidation. Prog Energy Combust Sci 1997;23:95–132.
[40] Tesner PA, Snegiriova TD, Knorre VG. Kinetics of dispersed carbon formation. Combust Flame 1971;17:253–60.
[41] Magnussen BF, Hjertager BH. On mathematical modeling of turbulent combustion with special emphasis on soot formation and combustion. Proc Combust Inst 1976;16:719–29.
[42] Lindstedt PR. Simplified soot nucleation and surface growth steps for non-premixed flames. In: Bockhorn H, editor. Soot formation in combustion mechanisms and models. Berlin: Springer; 1994. p. 417–41.
[43] Frenklach M, Wang H. Detailed modeling of soot particle nucleation and growth. Proc Combust Inst 1990;23:1559–66.
[44] Kent JH, Wagner HGg. Why do diffusion flames emit smoke? Combust Sci Tech 1984;41:245–69.
[45] Reilly PTA, Gieray RA, Whitten WB, Ramsey JM. Direct observation of the evolution of the soot carbonization process in an acetylene diffusion flame via real-time aerosol mass spectrometry. Combust Flame 2000;122:90–104.
[46] Reilly PTA, Gieray RA, Whitten WB, Ramsey JM. Fullerene evolution in flame-generated soot. J Am Chem Soc 2000;122:11596–601.
[47] Bonczyk PA. In-situ optical measurement of additive effects on particulates in a sooting diffusion flame. Combust Flame 1983;51:219–29.
[48] Delichatsios MA. A phenomenological model for smoke-point and soot formation in laminar flames. Combust Sci Tech 1994;100:283–98.

[49] de Ris J. A scientific approach to flame radiation and material flammability. Fire safety science—Proceedings of the second international symposium, 1989. p. 29–46.
[50] Hwang JY, Chung SH. Growth of soot particles in counterflow diffusion flames of ethylene. Combust Flame 2001;125:752–62.
[51] Zelepouga SA, Saveliev AV, Kennedy LA, Fridman AA. Relative effect of acetylene and PAHs addition on soot formation in laminar diffusion flames of methane with oxygen and oxygen-enriched air. Combust Flame 2000;122:76–89.
[52] Xu F, El-Leathy AM, Kim CH, Faeth GM. Soot surface oxidation in hydrocarbon/air diffusion flames at atmospheric pressure. Combust Flame 2003;132:43–57.